Nanoscale

PAPER

View Article Online
View Journal | View Issue

Cite this: *Nanoscale*, 2024, **16**, 2983

Improving the development of human engineered cardiac tissue by gold nanorods embedded extracellular matrix for long-term viability†

Alberto Sesena-Rubfiaro, *[a] Navin J. Prajapati,[a] Lihua Lou,[b] Govinda Ghimire,[a] Arvind Agarwal[b] and Jin He *[a,c]

A myocardial infarction (MI), commonly called a heart attack, results in the death of cardiomyocytes (CMs) in the heart. Tissue engineering provides a promising strategy for the treatment of MI, but the maturation of human engineered cardiac tissue (hECT) still requires improvement. Conductive polymers and nanomaterials have been incorporated into the extracellular matrix to enhance the mechanical and electrical coupling between cardiac cells. Here we report a simple approach to incorporate gold nanorods (GNRs) into the fibrin hydrogel to form a GNR-fibrin matrix, which is used as the major component of the extracellular matrix for forming a 3D hECT construct suspended between two flexible posts. The hECTs made with GNR-fibrin hydrogel showed markers of maturation such as higher twitch force, synchronous beating activity, sarcomere maturation and alignment, t-tubule network development, and calcium handling improvement. Most importantly, the GNR-hECTs can survive over 9 months. We envision that the hECT with GNRs holds the potential to restore the functionality of the infarcted heart.

Received 27th October 2023,
Accepted 16th January 2024

DOI: 10.1039/d3nr05422e

rsc.li/nanoscale

Introduction

MI continues to be the leading cause of morbidity worldwide.[1] This condition can result in the loss of ~25% of 2–4 billion CMs present in the left ventricle.[2] A major challenge in the recovery of MI lies in the limited ability of CMs to proliferate coupled with the formation of non-conductive fibrotic scar. These scars contribute to ventricular dysfunction and disrupt the normal electrical coupling between the remaining viable CMs, further complicating the healing process.[3,4] Due to the scarcity of donors and significant complications associated with heart transplantations, alternative approaches such as cell-based therapies[5–7] and tissue engineering[8–10] have emerged as promising strategies for the treatment of MI. Among these, tissue engineering has demonstrated the potential to recapitulate the essential characteristics of the native myocardial environment, including topographical, mechanical properties, and extracellular features.[11–13] Nevertheless, this field still encounters notable obstacles in developing tissue constructs that adhere to specific design criteria necessary for optimal outcomes. These criteria include achieving appropriate stiffness, flexibility,[14] and pore size of constructs to facilitate cell integration and nutrient exchange.[15] Overcoming these challenges, however, holds great promise for enhancing MI treatment outcomes.

To overcome these challenges, hydrogels have emerged as a promising avenue to achieve cardiac regeneration due to their biocompatibility, tunable biodegradation rates, the capability to absorb and retain body fluids, and the ability to modify their chemical structure by using diverse substrate materials and crosslinking methods.[16] Moreover, the mechanical properties of the hydrogels can be precisely tuned to influence the biological function of CMs, thus offering additional control over the regulation process.[17] Various naturally-derived biomaterials, including fibrin,[18] collagen,[19,20] gelatin[21] and extracellular matrix (ECM)-based materials, have been widely used to enhance retention, survival and engraftment of tissue constructs. These biomaterials serve as scaffolding to facilitate revascularization.[22] Additionally, synthetic materials such as poly(ethylene glycol) (PEG)-based copolymers,[23–25] polylactic-

[a]*Department of Physics, Florida International University, Miami, FL 33199, USA. E-mail: jinhe@fiu.edu*
[b]*Department of Mechanical and Materials Engineering, Florida International University, Miami, FL 33174, USA*
[c]*Biomolecular Science Institute, Florida International University, Miami, FL 33199, USA*

†Electronic supplementary information (ESI) available: Materials and methods, GNR synthesis and surface functionalization, preparation and characterization of fibrin and GNR-fibrin, cardiac differentiation of hiPSC, fabrication of millitug device, formation of hECT with and without GNRs, twitch force measurements, immunofluorescence imaging of sarcomere structure, imaging of calcium transients, transmitted light bright field and dark field microscope images of the hECT, cross-sectioned hECT slices, data analysis. See DOI: https://doi.org/10.1039/d3nr05422e

co-glycolic acid (PLGA),[26,27] polycaprolactone (PCL),[28,29] *etc.* have been used for similar purposes. Although these hydrogels have offered ECM-like microenvironment to support cardiac cell functions, their nanoscale architectural and electrical properties fall short compared to the characteristics of the native myocardium.[30]

Moreover, while some studies have explored the delivery of non-conductive biomaterials through injectable hydrogels or transplantable cardiac patches, challenges persist. These challenges include limitations such as restricted cell–cell coupling and delayed electrical signal propagation across the infarcted myocardium, consequently preventing the synchronization of contracting CMs within the scar zone.[31] Recent studies have demonstrated that employing metallic nanomaterials offers a potential solution to address the current limitations associated with conventional hydrogel-based scaffolds (*e.g.*, drug delivery, stiffness, and conductivity).[32,33] By incorporating metallic nanomaterials, such as gold nanoparticles (GNPs), it is possible to enhance the performance of scaffolds in tissue engineering and regenerative medicine applications. GNPs have gained considerable attention due to their biocompatibility, ease of fabrication, and unique electrical and optical characteristics. They have been shown as promising nanomaterials for biomedical-related applications from imaging to diagnostics.[34,35] Several studies have explored the incorporation of GNP into scaffolds, including alginate-chitosan,[36] poly (e-caprolactone),[37] gelatin methacrylate (GelMA) UV-crosslinked hydrogel layer of cardiac tissue patch,[38] and decellularized omental matrix.[39] These studies have demonstrated significantly enhanced cell adhesion, proliferation, and viability.

In this study, we have successfully developed gold nanorods (GNRs)-fibrin hydrogel that exhibits enhanced mechanical and electrical properties. Using this hydrogel as the major component of ECM, a millimeter size hECT construct suspended between two flexible PDMS posts (referred to hereafter as a milli-tug device) are created from human induced Pluripotent Stem Cell (hiPSC)-CMs. Surprisingly, the hECTs with GNRs (GNR-hECT) have an impressive lifespan for over 9 months compared to the significantly shorter survival period of less than 1 month observed in the constructs without GNRs. We have conducted a series of studies to investigate the changes of tissue geometry and cell morphology, sarcomere organization, t-tubule expression, twitch force, beating and calcium handling. Noticeable structural and functional improvements have been observed within the GNR-hECT.

Jin He

Dr Jin He is an associate professor in the Physics Department and biomolecular science institute of Florida International University (FIU) at Miami, USA. He received his B. S. degree in Physics from Fudan University in 1999, and his Ph.D in Biophysics from Arizona State university (ASU) in 2005 (Supervisor: Prof. Stuart Lindsay). He served as a postdoctoral fellow from 2005 to 2007 and as an Assistant Professor research from 2007 to 2011 at the biological design Institute of ASU. In 2011, he joined FIU as assistant professor. His primary research interest focuses on molecular junctions, single molecule cellular biophysics, and nanobiotechnology.

Materials and methods

Surface functionalization of GNRs

We prepared cetyltrimethylammonium bromide (CTAB) stabilized GNRs with long axis mean size 72.3 nm and short axis mean size 16.8 nm (see the inset image in Fig. 1a and Fig. S1†). The details of GNR synthesis can be found in ESI.† The GNR surface functionalization is summarized in two steps (see Fig. 1a). In the first step, GNR-CTAB solution (0.342 mg, 5 mL) was centrifuged 10 min at 14 000 rpm then the top CTAB solution was decanted, leaving the GNR pellet at the bottom of the centrifuge tube. Deionized water was added to the tube and the solution was centrifuged again for 5 min at the same speed. The final supernatant was carefully decanted. The GNR pellet was resuspended in COOH-mPEG5K-SH solution (5 mM in deionized water) and left in the dark overnight at room temperature. On the next day, the GNR solution was centrifuged 5 min at 10 000 rpm to remove the excess of COOH-mPEG5K-SH. In the second step, coupling agents *N*-(3-dimethylaminopropyl)-*N*′-ethylcarbodiimide hydrochloride (EDC HCl, 5 mM) and *N*-hydroxysuccinimide (NHS, 5 mM) in 2-(*N*-morpholino) ethanesulfonic acid (MES, 500 mM) buffer were added to the tube containing GNR pellet and left for 3 hours at 4 °C. To remove MES and EDC/NHS, the GNR solution was centrifuged for 5 min at 10 000 rpm. The pellet was resuspended with deionized water at 20 °C and the pH was adjusted to 8.0 with NaOH (1 M). Poly-L-lysine solution (PLL, 0.1%, 2 : 1 w/v) was added to the GNR solution and left for 2 hours at 4 °C. To remove the PLL, the GNR solution was centrifuged for 5 min at 5000 rpm. Then the pellet was resuspended in deionized water (500 μL). Finally, the GNR-SH-PEG-COOH-NH2-PLL solution was stored at −20 °C for further use. Fig. S1c† shows the extinction spectra of GNR before and after PEG modification, as well as following PLL functionalization.

Preparation and characterization of fibrin and GNR-fibrin

Fibrin hydrogel was prepared by mixing 24.6 μL of human fibrinogen (Sigma, F3879, 25 mg mL^{-1}) with 4 μL of human thrombin (Sigma, 605190-M, 100 U mL^{-1}) at room temperature. To produce the GNR-fibrin hydrogel, 26 μL of GNR-SH-PEG-COOH-NH2-PLL solution was mixed with 20 μL of human thrombin (20.8 U mL^{-1}). Subsequently, 24.6 μL of human fibrinogen was added to the mixture, which was stirred

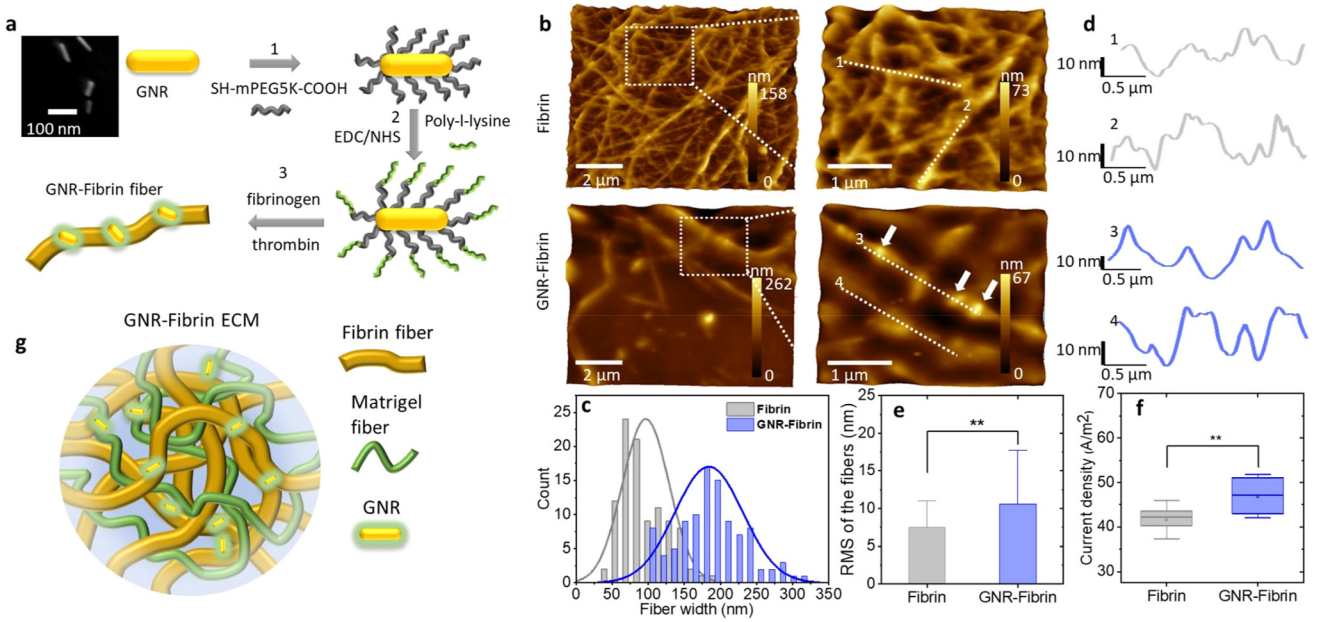

Fig. 1 GNR-Fibrin preparation. (a) Schematic diagram of GNR surface functionalization and GNR-fibrin hydrogel formation. The inset is the SEM image of GNRs. (b) AFM images of fibrin (top row) and GNR-fibrin (bottom row) fibers. The images on the right side are the zoom-in images in the regions enclosed by the white dashed squares in the images at the left side. The white arrows indicate the locations of GNR on a fibrin fiber. (c) The width distributions of the fibrin (gray) and GNR-fibrin (blue) fibers. The solid lines are the Gaussian fits. (d) Height profiles are through the white dashed lines marked in (b). The wavy background has been removed. (e) The RMS roughness of individual fibers of both fibrin and GNR-fibrin. The error bar is the standard deviation of 20 measurements. (f) The current density of the fibrin and the GNR-fibrin hydrogel. The error bar is the standard deviation of 20 measurements. The ANOVA test ($P \leq 0.05$) confirmed statistically significant differences in the current density. (g) Illustration of the GNR-fibrin based ECM composed of GNR-fibrin and Matrigel fibers.

thoroughly and carefully without introducing bubbles. Considering the charge polarity of thrombin and fibrinogen, we expect the positively charged PLL coating of GNR will interact stronger with the negatively charged fibrinogen through the electrostatic interactions. The PLL coated GNRs are also expected to stay on the negatively charged fibrin fiber.

The morphology of fibrin and GNR-fibrin fibers were examined by atomic force microscopy (Nanosurf FLexAFM, Liestal, Switzerland). Before imaging, 20 μL of hydrogel was deposited on a clean cover glass and dried at room temperature. Dyn190Al cantilevers with a resonant frequency of 190 kHz, nominal spring constant of 48 N m^{-1}, and tip radius <10 nm were used. The AFM images were acquired using a lateral scan speed of 0.78 s per line in the dynamic force mode (tapping mode) controlled by Nanosurf C3000 software (see Fig. 1b and Fig. S2†). Image analysis was performed using the Gwyddion software. To determine the width of fibrin fibers, we measured 20 spots per image and 5 images per sample. The root-mean-square (RMS) roughness values were calculated from individual fibers of both fibrin and GNR-fibrin. Prior to determining the RMS of individual fibers, wavy baselines of the height profiles were removed. The examined fibers were approximately 2–2.5 μm in length. Two samples and three images per sample were selected for the analysis. The current density of fibrin and GNR-fibrin hydrogels was acquired by measuring the electrical current through hydrogel per cross-section area with the same distance between electrodes.[40]

Cardiac differentiation of hiPSCs

The timeline of hiPSCs differentiation is illustrated in Fig. S4.† The hiPSCs from reprogrammed fibroblasts (GM23338, Coriell Institute for Medical Research, NJ, USA) were stored in liquid nitrogen until use. After defrosting, cells were cultured according to a previously reported protocol.[41] Briefly, hiPSCs were cultured on Matrigel-coated plates (BD Biosciences) with stem basal medium (mTeSR1, STEMCELL Technologies) for about 5 days to reach 90% of confluence. On day 0, hiPSCs were treated with 12 μM CHIR99021 (Tocris, 4423) diluted in RPMI/B27 minus insulin for 24 hours. On day 3, hiPSCs were treated with 5 μM IWP4 (Tocris, 5214) mixed with RPMI/B27 minus insulin, removed on day 4. The medium was replaced every other day. From day 8, hiPSCs were maintained in RPMI/B27 with insulin with regular media changes. Spontaneous contractions were observed between days 10 to 12. Following the previously reported protocol[42] to remove the excess of non-cardiomyocytes, the hiPSC-CMs were treated with 5 mM L-lactate (Sigma, 71718) diluted in RPMI without glucose (Gibco, 11879-020), for 2 days without media change until the day of the formation of the hECTs.

Formation of hECTs with and without GNRs

Purified hiPSC-CMs were dissociated from the substrate by TrypLE Express solution (Gibco) at 37 °C for 15 min. The detached cells were collected by centrifugation at 1400 rpm for 6 min. To form hECTs without GNR, each PDMS milli-tug device was loaded with 200 000 cells in a suspension of 2 μL RPMI/B27, 1.23 μL of human fibrinogen (Sigma, F3879, 25 mg mL^{-1}), 0.2 μL of human thrombin (Sigma, 605190-M, 100 U mL^{-1}), and 0.6 μL of Matrigel (Corning, 356230). The formation of GNR-hECTs proceeded through a two-step process. First, 1.3 μL of GNR-SH-PEG-COOH-NH2-PLL solution was mixed with 1 μL of human thrombin (20.8 U mL^{-1}), referred to as "solution A". Second, a suspension containing 200 000 cells was prepared in a mixture of 3 μL of RPMI/B27, 1.23 μL of human fibrinogen and 0.6 μL of Matrigel. This mixture is named as "solution B". Subsequently, each milli-tug device was initially loaded with solution A and then solution B was added using a pipette. The solutions were carefully mixed to ensure the absence of bubbles (see Fig. S4b†).

Next, the devices were filled with RPMI/B27 containing insulin, 5 μM Y27632 (Tocris, 1254), 10% fetal bovine serum, and 0.033 mg mL^{-1} aprotinin (Sigma, A3428). The medium was changed every other day. The tissues without GNRs were formed from day 12, and spontaneous beating was observed between days 17–18. However, the tissues with GNRs were formed from day 12 and the spontaneous beating was observed between days 26–27. Synchronous contraction of the tissue required approximately two additional days.

Tissues without GNRs were formed with hiPSC-CMs encapsulated in the extracellular matrix, prepared with a fibrin-hydrogel solution composed of 25 mg mL^{-1} human fibrinogen, 3 μL Matrigel, and 100 U mL^{-1} human thrombin (Sigma, 605190M).

Fabrication of milli-tug device

Milli-tug devices (see Fig. S4†) were fabricated by first pouring uncured polydimethylsiloxane (PDMS, Dow Corning Sylgard 184, prepared at 25 : 1 ratio of base : curing agent) into a polypropylene plastic mold, which was then baked overnight at 70 °C. Before cell seeding, the milli-tug devices were sterilized by immersion in 70% ethanol for 30 minutes and exposure to UV-light for 20 minutes.[43] The surfaces of the device were treated with 4% Pluronic F127 to reduce cell adhesion. The final milli-tug device presents two posts with hemispherical caps of 0.39 mm diameter, 1.46 mm height, and 0.39 mm thickness.

Twitch force measurement

The spontaneous contraction force (twitch force) and the corresponding beating frequency were measured based on the deflection of flexible post top (Δx) in the milli-tug device, as previously described.[44] Briefly, assuming the post has uniform material properties and dimensions, each deflection reports the force contraction proportional to the post's spring constant. To calculate the twitch force (F), the spring constant (k) of the post was measured using the indentation setup (Hysitron Biosoft, Bruker, Billerica, MA) with a spherical probe of 400 μm diameter. We have found that the tissue can be located at the middle of the post from top to bottom. Therefore, the acquired spring constant k at the middle of the post was 4.47 ± 0.31 N m^{-1} based on five measurements in air. This value was used to calculate the twitch force F using hook's law $F = k\Delta x$.

Data analysis

The data analysis was accomplished with custom Matlab script used to estimate the twitch force of the hECTs and calcium transients. Results are reported as mean ± SD. ImageJ were used to assess the analysis of the sarcomere size of the fluorescence images. To compare the data groups, one-way ANOVA-test and Mann Whitney-test were employed with $P \leq 0.05$ considered significantly different. The Kaplan–Meier curves were constructed using number of tissues survived at different culture timepoints. The tissue is considered failure when the following conditions happen: (1) stop beating; (2) breaking apart or off the posts; (3) significant decrease in the width and thickness (>60%) or significant drop in the twitch force (>60%). To account for the tissues used for characterizations, we have included the loss of one tissue at each timepoint. All statistical analysis was performed using GraphPad 5.0.

Results and discussion

GNR-fibrin matrix

We prepared cetyltrimethylammonium bromide (CTAB) stabilized GNRs with long axis mean size 72.3 nm and short axis mean size 16.8 nm (see the inset image in Fig. 1a and Fig. S1†). The details of GNR synthesis can be found in ESI.† Fig. 1a illustrates the steps for GNR surface functionalization and GNR-fibrin hydrogel formation.

In step 1, to improve the stability of GNR and avoid the toxic effect of CTAB,[45] the CTAB layer of the GNR surface was replaced with a PEG coating. In step 2, the PEG layer was covalently connected to PLL, which was employed to attract fibrinogens to the GNR surface through electrostatic interactions. In step 3, the fibrinogens on the GNR surface react with thrombins to form GNR-fibrin fibers. The AFM topography images of pure fibrin and GNR-fibrin hydrogels are shown in Fig. 1b. Compared to the pure fibrin sample, the GNR-fibrin fibers generally show a larger diameter. Fig. 1c shows the distribution of the measured widths of the fibrin and GNR-fibrin fibers from the AFM images, which were 97 ± 32 nm and 184 ± 47 nm, respectively. However, the stiffness of fibrin fibers is mainly determined by the density instead of the diameter of fibers.[46] The GNR-fibrin fibers in the AFM images appear straighter, indicating an enhanced persistence length and reduced flexibility. Zooming-in images reveal the presence of GNRs on the fibrin fiber surface, which is consistent with the height profiles shown in Fig. 1d. We further conducted RMS roughness analysis based on the height profiles of individual

fibrin and GNR-fibrin fiber surfaces. As depicted in Fig. 1e, the fibrin fibers exhibited an average RMS roughness of 5.6 ± 1.6 nm, whereas the GNR-fibrin displayed a notably higher value of 9.6 ± 3.6 nm. The presence of GNPs on the fibrin fiber surface may help to densify the fiber and enhance fiber stiffness.

In addition to the morphological changes, we performed electrical measurements on fibrin and GNR-fibrin hydrogels to eliminate the potential influence of other conductive proteins within the hydrogel. As shown in Fig. 1f, the GNR-fibrin exhibits a slightly higher current density.

To create a CM friendly environment, we prepared GNR-fibrin based ECM (Fig. 1f) by further adding Matrigel (see S1†), which comprises laminin for adhesion and collagen IV for structural support. Laminin facilitates CM attachment and spreading, while collagen IV forms a 3D scaffold for tissue organization and maturation. Additionally, entactin and perlecan in Matrigel contribute to signalling pathways and ECM stability, creating a supportive milieu that encourages the CM growth and function.[47] We have observed significant improvement in the synchronization of calcium transients when a two-dimensional (2D) layer of CMs interacting with the GNR-fibrin based ECMs (see Fig. S3†), which may contribute to the improved coupling between CMs due to the improved mechanical and electrical properties of ECM. We then move on to build the three-dimensional (3D) constructs of CMs.

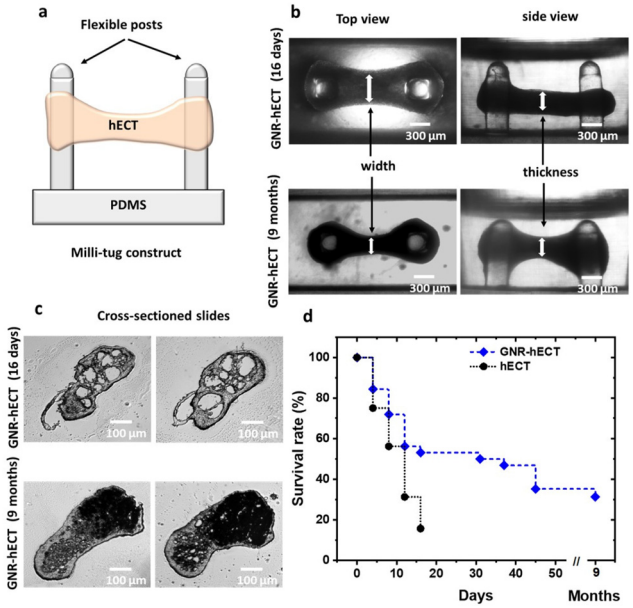

Fig. 2 Tissue formation. (a) Illustration of the hECT in the milli-tug construct. (b) Transmitted light microscope images (top and side views) of live GNR-hECTs cultured after 16 days (top row) and 9 months (bottom row) in the milli-tug construct. (c) Cross-sectioned slides of the GNR-hECTs of 16 days (top row) and 9 months (bottom row). (d) Kaplan–Meier survival curve of the hECTs with and without GNR over 9 months of culture. Significant differences were found at the time to compare the curves, $P = 0.0057$.

GNR-hECT long-term viability

We successfully fabricated hECTs in a milli-tug formation through self-assembly using the GNR-fibrin based ECM (see Fig. S4a†). The formed hECT is suspended between two flexible posts and under the static stress (see Fig. 2a and b). Interestingly, the self-assembly process of hECTs with GNRs occurred at a noticeably slower rate compared to the hECTs without GNRs. It took ~15 days for the hECTs with GNRs to develop spontaneous contractions, while GNR-free hECTs achieved this in ~6 days. This delay is attributed to the stiffer and larger GNR-fibrin fibers, and reduced mobility of the CMs inside the GNR modified ECM. To confirm the presence of GNRs within the hECTs, dark-field microscope images were obtained, revealing an increase in scattered light due to the presence of GNRs (see Fig. S4b†). This provides further evidence of the successful incorporation of GNRs within the hECTs.

Surprisingly, we observed that the GNR-hECT demonstrated remarkable longevity. As shown in Fig. 2d, typical hECT only lasts for about 16 days with a survival rate of ~50%, rarely exceeding 30 days. In contrast, more than 50% of the GNR-hECTs exhibited survival beyond 1 month and a subset of these constructs even persisted for 9 months (beyond which we did not conduct further testing). These findings align with previous reports where incorporating gold nanoparticles into ECM scaffolds promotes cell survival and retention.[35,48,49] Fig. 2b shows representative optical transmission images (side and top views) of the GNR-hECTs at day 16 and 9 months. The dumbbell shape of the tissue becomes more obvious after 9 months in comparison to its early shape at day 16. The middle section is smaller while the circular sections surrounding the two PDMS posts are enlarged. Fig. 2c shows the representative transmitted light microscope images for the thin tissue cross-section slides at day 16 and 9 months. Notably, on day 16, the two slides present several conspicuous voids. In contrast, the occurrence of voids is less frequent, and their size is significantly smaller in the normal hECTs without GNRs (see Fig. S4b†). These voids likely reflect the diminished fluidity of the larger GNR-fibrin fibers and the decreased mobility (coupled with stronger adhesion) of the CMs within the GNR-fibrin ECMs. This observation aligns with the decelerated self-assembly process. Therefore, the GNR-fibrin ECMs contributes to the formation of a 3D structure characterized by increased porosity with the presence of large voids, which are beneficial for the growth of cells.[15] Interestingly, in the 9-month-old tissues, these prominent voids disappear, replaced by darker regions that appear opaque to the transmitted light. These regions have a higher density, likely indicating the presence of CMs in the voids. As shown, we observed the healthy growth of CMs both from the outside morphology (Fig. 2b) and interior structural changes (Fig. 2c) of the GNR-hECT. Hence, the existence of large voids facilitates the penetration of culture medium into the interior of tissue, promoting the efficient delivery of oxygen and nutrients to all the CMs, which are critical for the survival and growth of

CMs.[50,51] These remarkable and exciting structural transformations strongly suggest that the presence of GNR in the ECM is beneficial for the growth and maturation of hiPSC-CMs within the hECT.

GNR-hECT geometrical change

As shown in Fig. 2, the hECTs underwent noticeable geometrical changes at the macro scale. To quantify these changes, we measured the cross-section width and thickness in the middle section of the dumbbell-shaped hECTs, as indicated by the white arrows in the optical images in Fig. 2a. The changes are summarized in Fig. 3. Over a 16-day culture period, the hECT without GNR showed a continued reduction of both cross-section width and thickness from 575.1 ± 23.0 μm to 479.1 ± 18.4 μm and 381.3 ± 21.8 μm to 310.7 ± 16.4 μm, respectively (Fig. 3a and b). In contrast, GNR-hECT experienced only minor changes in the width and thickness over the same period. As shown in Fig. 3c and d, the width and thickness of the hECT are consistently smaller than that of GNR-hECT and the differences are enlarged over time. The bigger size of GNR-hECT is consistent with its porous structure with large voids. In addition, the 9 months old GNR-hECTs showed significant size variations, reflecting the differences of tissue development over long time. We expect this can be further improved after optimizing the growth conditions. Additionally, the morphology of individual CMs within the hECT plays a role in determining the overall shape and size of the tissues. We have isolated individual cells from hECT of day 16 using papain enzyme (see S8†).[9] The isolated cells from tissue without GNR showed significant variations in size and shape. In contrast, the cells from the GNR-hECT showed uniformly elongated shapes and were generally bigger in size, suggesting a higher degree of maturation (see Fig. S7†).

Twitch force

The healthy hECT beats spontaneously. We measured the contraction force (twitch force) and beating frequency of the hECT with and without GNRs at different days of culture. Fig. 4a shows the typical recordings of the twitch force time traces for tissues after 4 days of culture, highlighting the incomplete electromechanical couplings between CMs in the tissue during the early stage. On day 16, the twitch force magnitude of the normal hECTs without GNRs decreases significantly (Fig. 4b), indicating tissue deterioration nearing the end of their lifespan. In contrast, the GNR-hECTs beat even stronger. Further, the GNR-hECTs continue to demonstrate robust beating on day 31, day 45, and even after 9 months (Fig. 4c). Fig. 4d summarizes the trend of twitch force magnitude *versus* culture time for both types of tissues. For the hECTs without GNRs, the twitch force magnitude peaks near day 12 and noticeably declines by day 16. Conversely, the force magnitude of the GNR-hECTs increases continuously to day 31 then remains consistently high for an extended duration. Following a 9-month culture period, there was a noticeable decrease in the magnitude of force generated by the GNR-hECTs, which can be attributed to Cell–ECM remodeling. However, despite this decrease, the force level remains relatively high. It should be

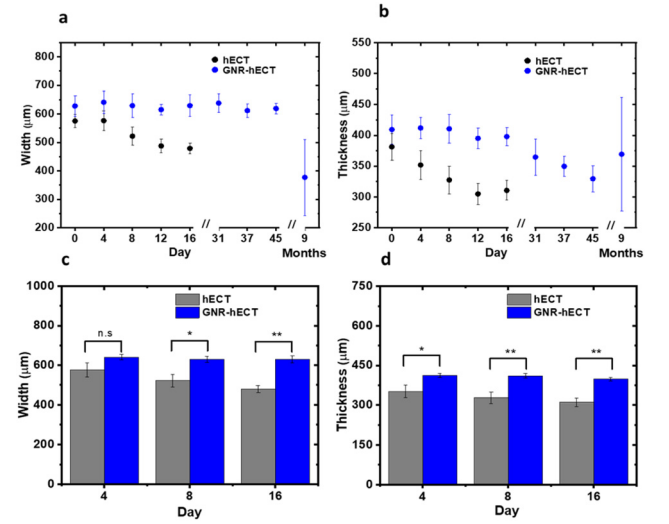

Fig. 3 Geometrical changes of the hECT with and without GNR. (a and b) The changes of the cross-section width (a) and thickness (b) of the hECTs *versus* culture time. (c and d) Comparation of the sizes of hECT with and without GNRs on the first 16 days of culture. The error bars are calculated from the standard deviation of 5 different hECTs.

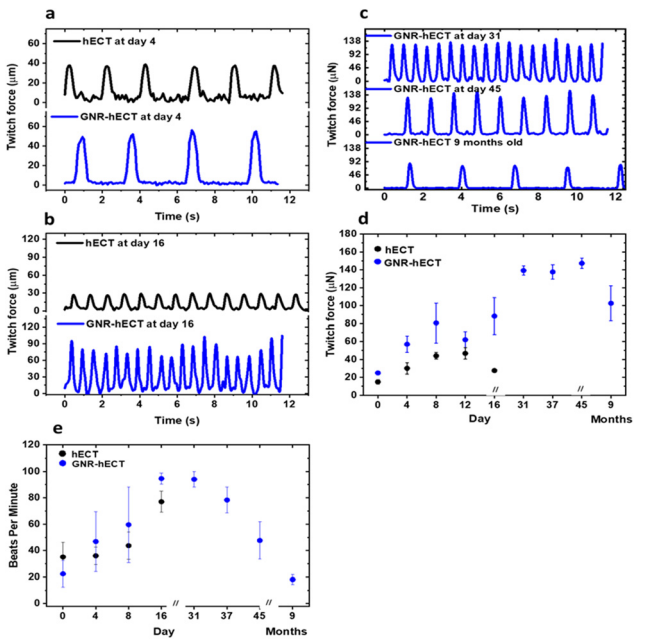

Fig. 4 Twitch force and beating rate of the hECTs with and without GNRs. (a and b) Typical twitch force-time traces without (black color) and with GNRs (blue color) at day 4 (a) and day 16 (b). (c) Twitch force-time traces at day 31 and 45, and 9 months of culture. (d and e) The twitch force and beating rate as a function of culture time for hECTs with and without GNR's. The error bars are calculated from the standard deviation of 6 different hECTs per day.

noted that the mechanical properties of the PDMS posts where the GNR-hECT was anchored might also alter over long time,[52,53] contributing to the variations. Fig. 4e compares the beating rate of the hECTs with and without GNR. Overall, the beating rate of GNR-free hECTs is slightly lower than that of the GNR-hECTs. During the initial 16 days of culture, the higher beating rate observed in the GNR-hECTs may be attributed to the expression of the arrhythmia commonly associated with immature CMs within the tissues. The continuous decrease of spontaneous beating rate after one month of culture potentially

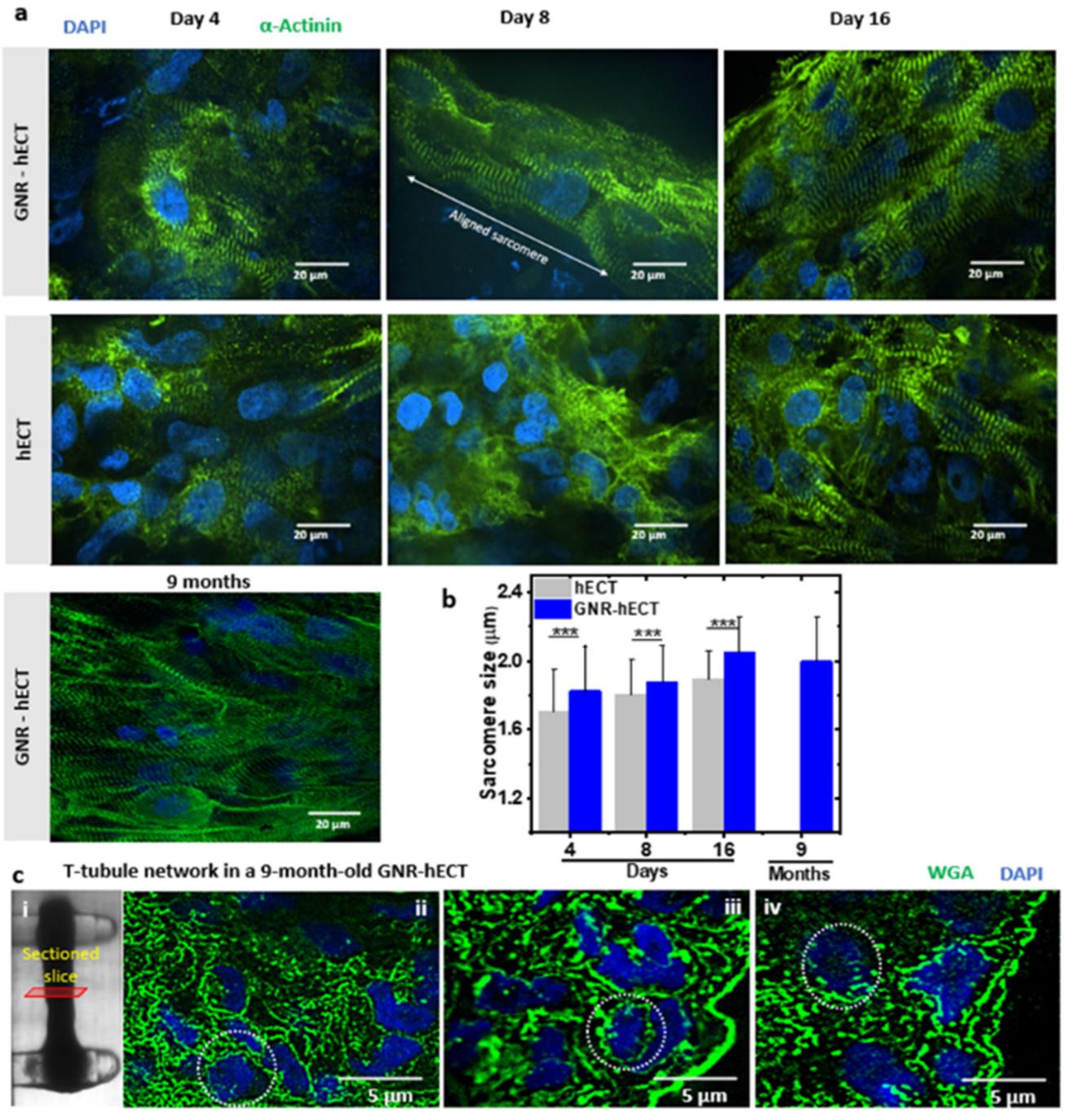

Fig. 5 Sarcomere and t-tubule structures of the hECTs with and without GNR. (a) Representative immunostained images of the structural organization in the GNR-hECT (first row) and hECT (second row) stained for α-actinin (green) and nucleus (blue). (b) Statistical analysis of the sarcomere size for the hECT without and with GNR. Significant differences of the sarcomere size were confirmed by ANOVA test ($N = 3$, $P < 0.05$). (c) (i) Bright field transmitted light image of a GNR-hECT cultured after 9 months in the milli-tug construct. (ii–iv) Three representative fluorescence images of cross-sectioned slices from the tissue stained with WGA (green) showing the formation of the t-tubule network (green) and nuclei (DAPI, blue) at the center (ii) and near the edges of the tissue (iii and iv). The regions enclosed by the white dotted circles clearly show the t-tubule network.

indicates the higher degree of maturation of the GNR-hECTs with a better electrical coupling between CMs.

The contractility of tissues is expected to be affected by their stiffness and geometry. We have performed non-invasive indentation experiments to compare the mechanical properties of tissues at the early stage. In the first 16 days, the GNR-hECTs consistently show a higher mean Elastic modulus than that of hECTs (see S8 of the ESI† for more details). The presence of GNRs likely stiffens the ECM and alters the mechanical environment of tissues, thus impacting CM morphology, alignment, and contractility. The higher twitch force of GNR-hECTs achieved after one month of culture likely due to an increase in cell–cell coupling and the denser CM packing. The higher density facilitates more efficient force transmission within the tissue, translating to enhanced contractility.

We also studied the intracellular calcium handling of the hECTs loaded with Fluo-4. The calcium transients from the hECTs without GNRs generally show a bigger variation in their shape compared to the more uniform transients from GNR-hECTs (Fig. S5a†). The difference also reflects the better electrical couplings between CMs in the GNR-hECTs. The mean width of the calcium transients also shows a robust increase for the GNR-hECTs from day 4 to day 11 of culture (Fig. S5b†). The improvement in calcium handling potentially facilitates the maintenance of a higher concentration of intracellular calcium, leading to a stronger contraction with a bigger twitch force.

Sarcomere maturation

We further investigate the sarcomere organization of the interconnected hiPSC-CMs within the hECT with and without GNRs. Fig. 5a shows the representative immunofluorescence images of the hECT with α-actinin and nucleus staining at different culture time. Following an 8-day culture period, a notable elongation and alignment of the sarcomeres were observed within the GNR-hECT alongside the extended axis between two PDMS posts. Furthermore, after 9 months of culture, the GNR-hECTs showed more pronounced and better sarcomere alignment similar to that observed in mature myocardial tissue. We also conducted the statistical analysis of these images (see Fig. 5b). For the hECTs without GNRs, the sarcomere size increases from 1.7 ± 0.2 μm at day 4 to 1.9 ± 0.2 μm at day 16. For the GNR-hECTs, the size increases from 1.8 ± 0.3 μm at day 4 to 2.1 ± 0.2 μm at day 16, but slightly decreases to 2.0 ± 0.3 μm for the 9 months old hECT. The sarcomere size of the GNR-hECT is closer to the matured sarcomere length about 2.2 μm.[54] These results showed that GNR-fibrin ECM enhanced the sarcomere structure of CMs with better alignment, obviously increased length and long-term viability.

Furthermore, we analyzed the nuclei-to-sarcomeres volume ratio by examining the immunofluorescence confocal *z*-stack images (see Fig. S6a and b†). Comparing hECTs and GNR-hECTs on both day 4 and day 16, the ratio is lower for GNR-hECTs, suggesting a higher percentage of sarcomeres per cell for GNR-hECTs. For GNR-hECTs, the volume ratio displayed a substantial reduction following a 9-month cultivation period. This decrease indicates a enhanced development of sarcomeres, which is consistent with the structural improvement of sarcomeres. Meanwhile, the nuclei number within the *z*-stacks of the GNR-hECTs obviously increase after 9 months of cultivation (see Fig. S6d†). Therefore, the CM density increased clearly inside the GNR-hECTs after 9 months. The increase of CM density may be due to the reduced porosity of the tissue, the migration of CMs and the possible proliferation of CM. However, more experiments are needed to confirm the CM proliferation.

The t-tubule system is intricately connected to the interior sarcomere structure. To explore the progress of the t-tubule network development, we utilized WGA staining on thin cross-sectioned slices of 9-month-old GNR-hECTs (see Fig. 5c(i)). The t-tubule presented a network-like structure that penetrating deep from the surface (see Fig. 5c(ii–iv)). Overall, our results indicated a higher WGA intensity throughout the entire slice for GNR-hECTs, suggesting a better developed t-tubule system. The enhancements in t-tubule structure, as revealed by WGA fluorescence imaging, align with the improvements observed in twitch force and calcium handling measurements and sarcomere structure.

Conclusions

In summary, our study demonstrates the successful formation of GNR-fibrin hydrogel, which serves as the primary component of the ECM for generating 3D constructs of hiPSC-CMs known as hECTs within a milli-tug device. Compared to fibrin hydrogel, the GNR-fibrin hydrogel exhibits thicker fibers and slightly higher conductivity. The millimeter size GNR-hECTs formed using GNR-fibrin based ECM, have significantly improved lifespan. Throughout a 9-month culture period, we monitored the structural and functional changes of these hECTs. At the early time of maturation, the interior of GNR-hECT displayed higher porosity with large voids. After 9 months of culture, these voids were populated with cells. Array of methods, including immunofluorescence imaging of sarcomere structure, WGA staining to assess t-tubule network development, calcium handling recordings, and twitch force measurements have been employed to characterize the tissues. Overall, the GNR-hECTs showed a higher degree of maturation compared to the hECT without GNRs during the initial 16 days of culture. The better-developed membrane structures of the t-tubule system are consistent with the sarcomere structure development, enabling effective electrical signal propagation as revealed by the calcium handling measurements. Consequently, the GNR-hECT generates more prominent twitch force with a slightly higher beating frequency.

Based on our findings, the presence of GNRs improves the structural and mechanical properties of hECT and the couplings between CMs, thus promoting the synchronization, viability, motility and growth of CMs inside the hECT. The CMs in

GNR-hECTs may experience increased proliferation. However, fully mature CMs typically lack proliferative capacity. One possibility is that some stem cells and immature CMs remaining after cell purification are proliferating while mature CMs undergo myonodal maturation. This additional cell proliferation could benefit the maturation process by providing supplementary support and signalling factors. GNRs might also facilitate the differentiation of remaining iPSCs. Previous studies suggest metallic nanomaterials can influence the differentiation of mesenchymal stem cells into the cardiac lineage.[55–57] Moreover, GNRs may also activate cellular signaling pathways to induce an upregulation of gene expression[58–60] that can improve the cardiac maturation. Therefore, the presence of GNR may have multifaceted impacts on the maturation of cardiac tissues. Further investigations are needed to understand the mechanism and determine the most relevant properties of GNR fibrin-based ECM (*e.g.*, the structure, stiffness, electrical conductivity of ECM, and ECM-cell contact) that are crucial in inducing the remodeling and long-term viability of the GNR-hECT. Nevertheless, the GNR-fibrin hydrogel demonstrates promising potential for the advancement of the next-generation hECT in the rational designed 3D constructs and potential clinical applications in cardiac tissue transplants.

Author contributions

A.S.-R.: investigation, formal analysis, writing an original draft. N.J.P., L.L., G.G. J.H.: resources, methodology. A.A.: investigation, methodology, supervision. J.H.: investigation, methodology, supervision, conceptualization, funding, writing a draft.

Conflicts of interest

The authors declare no competing financial interest in association with this study.

Acknowledgements

We would like to acknowledge the contribution of Chris Chen's lab in sharing the protocols for culturing hiPSC cells and forming the hECT on the milli-tug device. We also extend our gratitude to Thomas Bifano's lab for sharing the method of twitch force measurement. This work was mainly supported by the ERC program of NSF under NSF Cooperative Agreement No. EEC-1647837. We also acknowledge using machines and electronic shops of FIU College of Arts, Sciences and Education (CASE).

References

1 *World health statistics: monitoring health for the SDGs, Sustainable Development Goals*. Geneva: World Health Organization, 2023, pp. 10–16.
2 C. E. Murry, H. Reinecke and L. M. Pabon, *J. Am. Coll. Cardiol.*, 2006, **47**, 1777–1785.
3 S. D. Prabhu and N. G. Frangogiannis, *Circ. Res.*, 2016, **119**, 91–112.
4 P. Menasché, A. A. Hagège, J.-T. Vilquin, M. Desnos, E. Abergel, B. Pouzet, A. Bel, S. Sarateanu, M. Scorsin and K. Schwartz, *J. Am. Coll. Cardiol.*, 2003, **41**, 1078–1083.
5 E. Cambria, F. S. Pasqualini, P. Wolint, J. Günter, J. Steiger, A. Bopp, S. P. Hoerstrup and M. Y. Emmert, *npj Regener. Med.*, 2017, **2**, 1–10.
6 K. R. Chien, J. Frisén, R. Fritsche-Danielson, D. A. Melton, C. E. Murry and I. L. Weissman, *Nat. Biotechnol.*, 2019, **37**, 232–237.
7 Y. Shiba, T. Gomibuchi, T. Seto, Y. Wada, H. Ichimura, Y. Tanaka, T. Ogasawara, K. Okada, N. Shiba and K. Sakamoto, *Nature*, 2016, **538**, 388–391.
8 T. Boudou, W. R. Legant, A. Mu, M. A. Borochin, N. Thavandiran, M. Radisic, P. W. Zandstra, J. A. Epstein, K. B. Margulies and C. S. Chen, *Tissue Eng., Part A*, 2012, **18**, 910–919.
9 K. Ronaldson-Bouchard, S. P. Ma, K. Yeager, T. Chen, L. Song, D. Sirabella, K. Morikawa, D. Teles, M. Yazawa and G. Vunjak-Novakovic, *Nature*, 2018, **556**, 239–243.
10 A. F. G. Godier-Furnémont, M. Tiburcy, E. Wagner, M. Dewenter, S. Lämmle, A. El-Armouche, S. E. Lehnart, G. Vunjak-Novakovic and W.-H. Zimmermann, *Biomaterials*, 2015, **60**, 82–91.
11 A. Patino-Guerrero, J. Veldhuizen, W. Zhu, R. Q. Migrino and M. Nikkhah, *J. Mater. Chem. B*, 2020, **8**, 7571–7590.
12 N. Annabi, K. Tsang, S. M. Mithieux, M. Nikkhah, A. Ameri, A. Khademhosseini and A. S. Weiss, *Adv. Funct. Mater.*, 2013, **23**, 4950–4959.
13 T. Eschenhagen, A. Eder, I. Vollert and A. Hansen, *Am. J. Physiol.: Heart Circ. Physiol.*, 2012, **303**, H133–H143.
14 S. L. Dahl, C. Rhim, Y. C. Song and L. E. Niklason, *Ann. Biomed. Eng.*, 2007, **35**, 348–355.
15 J. Zeltinger, J. K. Sherwood, D. A. Graham, R. Müeller and L. G. Griffith, *Tissue Eng.*, 2001, **7**, 557–572.
16 Q. Chai, Y. Jiao and X. Yu, *Gels*, 2017, **3**, 6.
17 A. Navaei, K. R. Eliato, R. Ros, R. Q. Migrino, B. C. Willis and M. Nikkhah, *Biomater. Sci.*, 2019, **7**, 585–595.
18 K. L. Christman, H. H. Fok, R. E. Sievers, Q. Fang and R. J. Lee, *Tissue Eng.*, 2004, **10**, 403–409.
19 S. Rinkevich-Shop, N. Landa-Rouben, F. H. Epstein, R. Holbova, M. S. Feinberg, O. Goitein, T. Kushnir, E. Konen and J. Leor, *J. Cardiovasc. Pharmacol. Ther.*, 2014, **19**, 470–480.
20 S. Pedron, S. van Lierop, P. Horstman, R. Penterman, D. J. Broer and E. Peeters, *Adv. Funct. Mater.*, 2011, **21**, 1624–1630.
21 M. Nikkhah, M. Akbari, A. Paul, A. Memic, A. Dolatshahi-Pirouz and A. Khademhosseini, *Biomaterials from nature for advanced devices and therapies*, 2016, pp. 37–62.
22 S. B. Seif-Naraghi, J. M. Singelyn, M. A. Salvatore, K. G. Osborn, J. J. Wang, U. Sampat, O. L. Kwan,

G. M. Strachan, J. Wong and P. J. Schup-Magoffin, *Sci. Transl. Med.*, 2013, **5**, 173ra125.
23 S. Bhutani, A. L. Nachlas, M. E. Brown, T. Pete, C. T. Johnson, A. J. García and M. E. Davis, *ACS Biomater. Sci. Eng.*, 2018, **4**, 200–210.
24 S. Dobner, D. Bezuidenhout, P. Govender, P. Zilla and N. Davies, *J. Card. Failure*, 2009, **15**, 629–636.
25 R. Komeri and J. Muthu, *J. Biomed. Mater. Res., Part A*, 2016, **104**, 2936–2944.
26 J.-P. Karam, C. Muscari, L. Sindji, G. Bastiat, F. Bonafè, M.-C. Venier-Julienne and N. C. Montero-Menei, *J. Controlled Release*, 2014, **192**, 82–94.
27 M. Patel, A. Jha and R. Patel, *J. Polym. Res.*, 2021, **28**, 214.
28 J. Chen, R. Guo, Q. Zhou and T. Wang, *Kaohsiung J. Med. Sci.*, 2014, **30**, 173–180.
29 T. Wang, X.-J. Jiang, Q.-Z. Tang, X.-Y. Li, T. Lin, D.-Q. Wu, X.-Z. Zhang and E. Okello, *Acta Biomater.*, 2009, **5**, 2939–2944.
30 M. Rienks, A.-P. Papageorgiou, N. G. Frangogiannis and S. Heymans, *Circ. Res.*, 2014, **114**, 872–888.
31 Z. Cui, B. Yang and R.-K. Li, *Engineering*, 2016, **2**, 141–148.
32 M. Yadid, R. Feiner and T. Dvir, *Nano Lett.*, 2019, **19**, 2198–2206.
33 H. Esmaeili, A. Patino-Guerrero, M. Hasany, M. O. Ansari, A. Memic, A. Dolatshahi-Pirouz and M. Nikkhah, *Acta Biomater.*, 2022, **139**, 118–140.
34 C. M. Cobley, J. Chen, E. C. Cho, L. V. Wang and Y. Xia, *Chem. Soc. Rev.*, 2011, **40**, 44–56.
35 Y. Li, X. Shi, L. Tian, H. Sun, Y. Wu, X. Li, J. Li, Y. Wei, X. Han, J. Zhang, X. Jia, R. Bai, L. Jing, P. Ding, H. Liu and D. Han, *Adv. Mater.*, 2016, **28**, 10230–10235.
36 N. E. Beltran-Vargas, E. Peña-Mercado, C. Sánchez-Gómez, M. Garcia-Lorenzana, J.-C. Ruiz, I. Arroyo-Maya, S. Huerta-Yepez and J. Campos-Terán, *Polymers*, 2022, **14**, 3233.
37 A. Shapira, R. Feiner and T. Dvir, *Int. Mater. Rev.*, 2016, **61**, 1–19.
38 A. Navaei, H. Saini, W. Christenson, R. T. Sullivan, R. Ros and M. Nikkhah, *Acta Biomater.*, 2016, **41**, 133–146.
39 M. Shevach, S. Fleischer, A. Shapira and T. Dvir, *Nano Lett.*, 2014, **14**, 5792–5796.
40 A. Sesena-Rubfiaro, N. J. Prajapati, L. Paolino, L. Lou, D. Cotayo, P. Pandey, M. Shaver, J. D. Hutcheson, A. Agarwal and J. He, *ACS Biomater. Sci. Eng.*, 2023, **9**, 1644–1655.
41 X. Lian, C. Hsiao, G. Wilson, K. Zhu, L. B. Hazeltine, S. M. Azarin, K. K. Raval, J. Zhang, T. J. Kamp and S. P. Palecek, *Proc. Natl. Acad. Sci. U. S. A.*, 2012, **109**, E1848.
42 S. Tohyama, F. Hattori, M. Sano, T. Hishiki, Y. Nagahata, T. Matsuura, H. Hashimoto, T. Suzuki, H. Yamashita, Y. Satoh, T. Egashira, T. Seki, N. Muraoka, H. Yamakawa, Y. Ohgino, T. Tanaka, M. Yoichi, S. Yuasa, M. Murata, M. Suematsu and K. Fukuda, *Cell Stem Cell*, 2013, **12**, 127–137.
43 W. R. Legant, A. Pathak, M. T. Yang, V. S. Deshpande, R. M. McMeeking and C. S. Chen, *Proc. Natl. Acad. Sci. U. S. A.*, 2009, **106**, 10097.
44 N. J. Sniadecki and C. S. Chen, in *Methods in Cell Biology*, Academic Press, 2007, vol. 83, pp. 313–328.
45 Y. P. Jia, K. Shi, J. F. Liao, J. R. Peng, Y. Hao, Y. Qu, L. J. Chen, L. Liu, X. Yuan, Z. Y. Qian and X. W. Wei, *Small Methods*, 2020, **4**, 1900799.
46 W. Li, J. Sigley, M. Pieters, C. C. Helms, C. Nagaswami, J. W. Weisel and M. Guthold, *Biophys. J.*, 2016, **110**, 1400–1410.
47 E. A. Aisenbrey and W. L. Murphy, *Nat. Rev. Mater.*, 2020, **5**, 539–551.
48 K. Roshanbinfar, M. Kolesnik-Gray, M. Angeloni, S. Schruefer, M. Fiedler, D. W. Schubert, F. Ferrazzi, V. Krstic and F. B. Engel, *Adv. Healthcare Mater.*, 2023, **12**, 2202408.
49 Y. Dong, M. Hong, R. Dai, H. Wu and P. Zhu, *Sci. Total Environ.*, 2020, **707**, 135976.
50 I. Yonatan, G. Mitchell, B. Kristen, W. Aaron, Z. Jinyun, N. Guangming, Z. Chao and A. Aitor, bioRxiv, 2020, DOI: **10.1101/2020.06.25.171611**, 2020.2006.2025.171611.
51 A. Kahn-Krell, D. Pretorius, B. Guragain, X. Lou, Y. Wei, J. Zhang, A. Qiao, Y. Nakada, T. J. Kamp, L. Ye and J. Zhang, *Front. Bioeng. Biotechnol.*, 2022, **10**, 908848.
52 K. Song, N.-K. Cho, K. Park and C.-S. Kim, *Polymers*, 2022, **14**(12), 2373.
53 D. Kumar and S. S. Singh, *IOP Conf. Ser.: Mater. Sci. Eng.*, 2022, **1225**, 012041.
54 E. Karbassi, A. Fenix, S. Marchiano, N. Muraoka, K. Nakamura, X. Yang and C. E. Murry, *Nat. Rev. Cardiol.*, 2020, **17**, 341–359.
55 P. Baei, S. Jalili-Firoozinezhad, S. Rajabi-Zeleti, M. Tafazzoli-Shadpour, H. Baharvand and N. Aghdami, *Mater. Sci. Eng., C*, 2016, **63**, 131–141.
56 S. Sridhar, J. R. Venugopal, R. Sridhar and S. Ramakrishna, *Colloids Surf., B*, 2015, **134**, 346–354.
57 K. Adibkia, A. Ehsani, A. Jodaei, E. Fathi, R. Farahzadi and M. Barzegar-Jalali, *Beilstein J. Nanotechnol.*, 2021, **12**, 786–797.
58 C. Grabinski, N. Schaeublin, A. Wijaya, H. D'Couto, S. H. Baxamusa, K. Hamad-Schifferli and S. M. Hussain, *ACS Nano*, 2011, **5**, 2870–2879.
59 J. Lee and B. H. Hwang, *Biotechnol. Bioprocess Eng.*, 2022, **27**, 213–220.
60 S. M. Sadraei, J. Kiani and B. Ashtari, *Int. J. Biol. Macromol.*, 2022, **206**, 511–520.